3D Reconstruction and Visualization of Microstructure Surfaces from 2D Images

D. Samak, A. Fischer (1), D. Rittel
Laboratory for CAD & Lifecycle Engineering
Dept. of Mechanical Engineering
Technion-Israel Institute of Technology
Haifa, Israel, 32000
meranath@technion.ac.il

Abstract

This paper describes a stereophotogrammetry method that reconstructs 3D microstructure surfaces from Scanning Electron Microscope (SEM) images. The microstructure surfaces are represented as 3D meshes with texture. The method's algorithm is based on the following stages: a) computing 3D points from 2D matched points; b) triangulating the 3D points into a 3D mesh; and c) mapping a 2D image as a texture on the surface. The textured 3D surface exhibits very realistic 3D microstructure surfaces for 3D visualization and engineering analysis. The performance of the proposed method has been analyzed and demonstrated on a variety of materials and complex geometries.

Keywords

Microstructure surfaces, Engineering analysis, Visualization

1 INTRODUCTION

This paper describes a new method that reconstructs 3D textured meshes for microstructure surfaces from SEM images. Until now, visualization methods have represented the macro shape using 3D meshes while representing the micro structure using 2D images [1].

With the new proposed method the macro-micro structure is represented simultaneously, thus providing better insight into the sample for 3D diagnosis and analysis [2]. The macro shape of the sample is represented by the 3D mesh structure, while the micro details are represented by the mapped image texture on the mesh. The method is based on the following Computer Aided Geometric Design (CAGD) techniques [3]: stereophotogrammetry, mesh reconstruction, texture mapping and segmentation. Following is an overview of the state of the art in each of these techniques.

1.1 Stereophotogrammetry

Stereophotogrammetry is used to reconstruct a 3D object from two stereo images [4]. Typically, image matching is applied to create DEM (Digital Elevation Mapping) maps [5], among them terrain mapping. Figure 1 demonstrates the process of photographing two images of an object. The camera parameters are the same for both images. The object in the second image is rotated with respect to that in the first image. As a result, a 3D point M of the object is represented by 3D points M1* (the original position) and M2* (the rotated position) in the SEM's local coordinate system. Hence, M has two different projections on the images, M1 and M2, according to the position of the object. The two points M1 and M2, the center of rotation O and the rotated angle α between the object positions are known. Therefore, computing the depth value Zm of point M with respect to a reference plane is straightforward and can be computed by the following equations (1) and (2).

$$disp=(x2 - x1)+x1(1-\cos\alpha) \quad (1)$$

$$Zm = disp / \sin\alpha \quad (2)$$

where the disparity *disp* is defined as the relative difference in pixels between the corresponding points M1 and M2 of the stereo images. The points x_1 and x_2 are the x coordinates of M_1 and M_2, respectively.

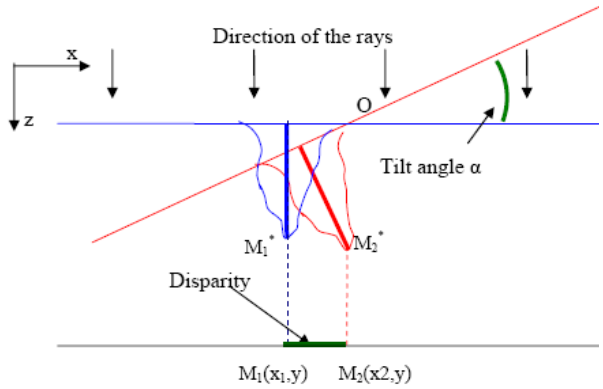

Figure 1: A scheme of the stereo images.

1.2 Delaunay Mesh Reconstruction

Stereophotogrammetry yields a cloud of 3D points that must be meshed to produce a 3D CAD model for visualization and analysis. The difficulty in meshing is especially apparent in complicated real 3D cases, where the triangulation (meshing with triangles) is not unique and evident [6]. Nonetheless, stereophotogrammetry is a 2.5D problem; hence, an object can be projected in 2D without loss of information. This meshing is much simpler than for 3D cases and is a well known problem (terrain mapping). The classical method of meshing a 2.5D cloud of points is to triangulate the points using the well known Delaunay triangulation method [7], as shown in Figure 2. In this way, the connectivity connections among the 3D points are determined by means of 2D triangulation on a plane.

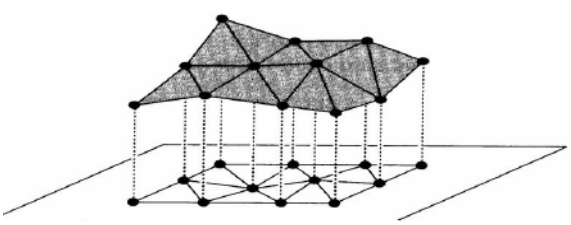

Figure 2: Triangulation of 2D projected points and the resulting 3D mesh.

1.3 Texture Mapping

Visualization of realistic 3D surfaces can be enhanced by applying texture mapping on the 3D mesh [8]. After reconstruction of the 3D mesh, the source image of the microstructure surface can be mapped onto the 3D mesh, thus combining the 3D representation with texture data. The new 3D image contains both macro information about the 3D shape and the micro structure of the texture. Though texture mapping is considered a complex problem [9], the current case is straightforward because of the geometry of the sample shape, characterized by genus-0 and a 2.5D cloud of points.

1.4 Texture Segmentation

Through texture segmentation, a particular region of the surface can be characterized, thus providing a better understanding for mechanical analysis. The common approaches for grayscale images are: threshold techniques [10], edge-based methods [11], active contour methods [12] and region-based techniques [13]. Following is a description of each approach:

Threshold techniques process local pixel information. They are effective when the intensity levels of the objects fall outside the range of the background levels. Nevertheless, blurred region boundaries can create disorder.

Edge-based methods focus on contour detection. Their weakness is in connecting broken contour lines, which are problematic in the case of blurring.

In the region-based method, the image is partitioned into connected regions with similar intensity levels. Then, adjacent regions are merged under a geometric or functional criterion. Constrained criteria, however, can create fragmentation, while tolerant criteria cause blurred boundaries.

Active contour methods are based on applying various shrink/expand operations on a given curve, according to an energy elastic function. These methods are commonly converged into a local minimum.

In the case of simple images, *threshold techniques* and *edge-based methods* can be easily adapted. For images with sharp feature boundaries, *active contour methods* are efficient. In the current case, *the region-based method* is most appropriate because of the particular complexity of the microstructure images.

2 APPROACH

The proposed method reconstructs 3D microstructure surfaces and represents them as textured 3D meshes. Consequently, a macro-micro structure can be represented simultaneously. The proposed method is based on the following stages:

a) Two images are taken by a SEM (Scanning Electron Microscope).
b) Initial photography parameters are pre-defined. A priori knowledge of the image features can improve the process.
c) The images are matched, and the 3D matched points are computed from the two stereo images.
d) The resulting 3D points are meshed, yielding a reconstructed 3D surface composed of triangles. A macrostructure is then defined.
e) The microstructure surface is defined by mapping a texture on the resulting 3D mesh.
f) The images are segmented to distinguish between different material deformed regions. This segmentation is marked on the 3D textured mesh.
g) Analyses and mechanical simulations, such as fracture analysis, can be applied by utilizing the 3D surface.

3 IMPLEMENTATION

Each of the approach stages was implemented and is described in detail in this section.

3.1 Stereo Matching

The stereo correlation algorithm is based on recognition of the matched points in two images, where one is tilted with respect to the other. The images are photographed by a SEM. In this implementation, the microstructure surface is laid on a platter. Then, the first image is photographed. Afterwards, the platter is rotated by about 5 to 10 degrees, and the second image is photographed.

Figure 3 describes the two different projections, M1 and M2, which are the projections of the same object point M photographed in two positions on stereo images. The differentiation is defined by the tilt angle α of the platter. Given that the center of rotation is at O(xo=0,yo=0), the depth Zm is given by equation (2).

In the stereo images, for each point M1 on the left image, a small window W1 is defined, with M1 as its center (the red window in Figure 3.a). The corresponding point of M1 in the second image, M2, is sought within a bigger window W2 (the blue window in Figure 3.b) around M1', which has the same coordinates as M1 in the right image.

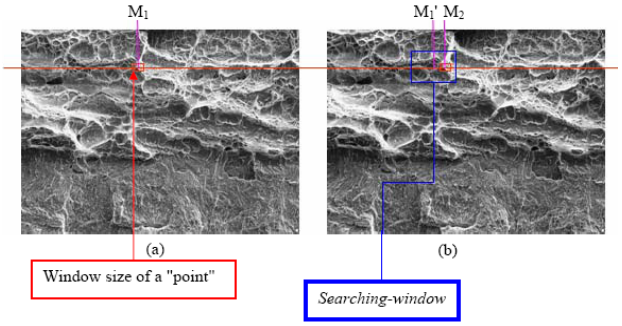

Figure 3: Matching two stereo images.

The size of the searching window W1 can be defined manually or can be generated automatically according to the texture complexity of the image. The more noisy the texture (high frequency), the smaller is the size of W1. The number of matched points is dictated by the image resolution and the window size of M1. When searching in the areas of W1 and W2, the best correlation of M1 to M2 is given by the following equation:

$$Min(x_2,y_2)\left\{\sum_{m=wsz/2}^{wsz/2}\sum_{n=wsz/2}^{wsz/2} I_1\left[\left(x_1+n,y_1+m\right)-\sum_{m=wsz/2}^{wsz/2}\sum_{n=wsz/2}^{wsz/2} I_2\left(x_2+n,y_2+m\right)\right]^2\right\} \quad (3)$$

where I1 is the left image and I2 is the right image; (x1,y1) is the reference point M1 of image I1, (x2,y2) is its correspondence point M2 at image I2 and W1sz is the window size of W1.

The following parameters should be defined for the matching algorithm:

- The X and Y offset of the images define the relative position between the images.
- The window sizes of W1 and W2 are in pixels.
- The scan threshold is defined as the width of the search band.
- The X-step and Y-step determine the density of the 3D computed points.
- The disparity threshold, eliminates the noise of Z values.

The stereo-matching algorithm is based on the following stages:

a) From the upper-left corner of the left image I1, select the first point M1 and compute the average intensity of the window.

b) Define a searching-window around the same coordinates of M1 in the right image I2.

c) Within this searching-window W2, search for the best correlation window corresponding to the reference point M1 using equation 3, and define its correspondence point M2.

d) Define the next reference point on X line (x1+step_x, y1), and repeat the same correspondence search.

e) For line y, go to the next reference point (x1, y1+step_y).

f) After finding all the correspondence points (M1,M2), compute the 3D point by triangulation, with the known tilt angle between the two images.

g) Compute the height Z of each point using equation 2.

h) Use the 3D points as a base for the triangulation process..

For an n×m image, the complexity of the algorithm is O(n m wsz). We assume in the algorithm that the two images are perfectly aligned, that is to say that the two corresponding points are on the same line y. But that assumption is not always valid, and sometimes the images have to be readjusted.

3.2 Meshing Reconstruction

The mesh is reconstructed by triangulating the 3D points. In our case, the points are in 2.5D according to the scanning technique of the SEM. In 2.5D, the object can be projected on a plane without any overlaps of the mesh elements. As a result, a 3D triangulation can be applied. Figure 4 demonstrates the 3D reconstruction process: (a) the reconstructed triangular mesh; (b) the shaded mesh (with facets); and (c) the textured 3D mesh.

The triangulation in 3D and 2D is not invariant; however, since the images are photographed from close positions, the neighboring relationships are preserved, and the 2D process is much simpler and more rapid.

3.3 Texture Mapping

To provide micro-details on the surface, texturing mapping of an image is applied on the 3D mesh. One of the input images is parameterized according to the 3D mesh, and each triangle of the image is projected on its corresponding triangle of the mesh. The result is a very realistic 3D surface represented by geometry and texture, making 3D macro-micro analysis possible. Figure 4.c shows a 3D surface with texture mapping. This macro-micro structure provides a better understanding of mechanical processes applied on 2D images.

3.4 Texture Segmentation

Through image segmentation, regions distinguished by their textures can be marked. Hence, different material properties can be extracted, and the impact of the mechanical processes that deformed the object can be recognized. The texture of microstructure surface images is complex. Therefore, classical segmentation algorithms from graphics and image processing fields that recognize functional surfaces or edges cannot be applied. Nevertheless, algorithms that classify texture patterns are more natural for segmentation of micro structures.

The desired segmentation for representing material deformation according to a fracture process is demonstrated in Figure 5. One of the leading algorithms for texture segments [13] was implemented and tested in this research. The main idea was to represent the image as a graph. The segments are represented by the nodes of the graph. Through a top-down process, properties of aggregates are accumulated at every scale of the image, from a single pixel up to the entire image. The algorithm takes into account some properties of segments, such as length, width, orientation and average intensity. The advantage in using such a graph is that it segments complex textured images, with each node then representing a segment. In our simulations, however, this algorithm was not sensitive to material deformations of our samples.

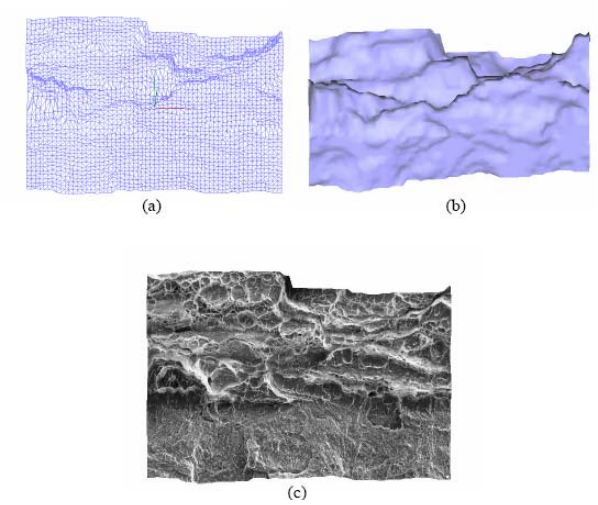

Figure 4: 3D reconstruction: (a) the 3D mesh; (b) the shaded mesh; and (c) the 3D mesh with texture.

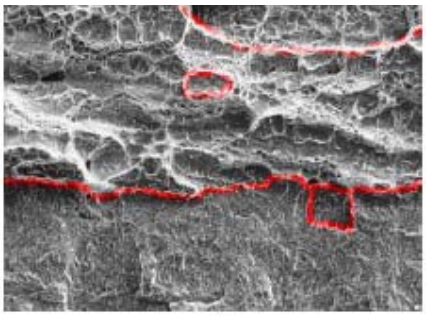

Figure 5: Texture segmentation.

4 PERFORMANCE ANALYSIS

This section demonstrates the feasibility of the proposed method for reconstructing 3D textured meshes through experiments on samples with different materials and simulation on synthetic geometric models of basic shapes and freeform surfaces. Three types of errors were measured: (a) the depth error (z value) with respect to the tilt angle; (b) the depth error (z value) with respect to SEM magnification; and (c) the depth error (z value) with respect to image disparity.

The depth error Δz with respect to the tilt angle: α is the tilt angle, and Zm is the height of the computed 3D point M with respect to a reference plane. Δz can be computed from equation 3:

$$\Delta z = \left\| \frac{\Delta z}{\Delta \alpha} \right\| = \left\| disp * \frac{\Delta \alpha}{\sin \alpha \tan \alpha} \right\| \quad (4)$$

In our case, the following values were defined: θ=10°, disp=100 pixel, and Δθ=0,05° = 8,73*10-4 rad. As a result Δz = **. The units of Δz depend on the scale defined, which can be in mm or in μm. The error εz is expressed as:

$$\varepsilon_z = \frac{\Delta z}{\langle z \rangle} \quad (5)$$

with $\langle z \rangle = \frac{disp}{\sin(\theta)}$ 575.9 *units*

Hence, the z-error due to the angle error of the SEM is less than 1%:

εz =0.495%.

The depth error with respect to SEM magnification:

Experimentation has shown that SEM magnification does not improve the computation results. For example, the MAGMA sample is magnified by ×2500. The main problem of magnification is due to mechanical tilting; at high magnification, the defects are increased and may cause undesired noise effects.

The depth error with respect to image disparity:

The error of the disparity resulting from the image resolution is about one pixel. For a common image, the resolution is 800x800 pixels. In such a case, the disparity error is: ε_{disp}=0.125%.

For θ=10° the disparity is: 1/sin(θ) = 5.76

where the depth error is: ε_2=0.72%

This error is the minimal error. The error is usually higher because of the distortion uncertainty.

4.1 Experiments of different materials

Three different samples of broken material were tested using our method, with the goal of analyzing the fracture behavior from the resulting 3D textured meshes. Each was tested on different SEM magnifications and different tilt angles. The three materials are: a) ceramic material; b) synthetic earth magma; and c) syntactic foam containing hollow glass spheres. The results of reconstructing textured 3D meshes from each of the above materials are demonstrated in Figure 6. The 3D shape provides more information of the surface roughness in areas with sharp gradients where the fracture occurred. Moreover, there is a strong correlation between the curvature changes of the 3D shape and the texture deformations.

Table 1 summarizes the characteristics of the material samples (ceramic material, synthetic magma and syntactic foam). The three examples were measured at a tilt angle of 10°. These materials were chosen because of their different textures. These examples indicate that the reconstruction algorithm works quite well for diverse material types. The foam texture is more regular and has a lower frequency. The Magma sample was studied at a higher magnification, and its reconstruction seems suitable. Three of the samples produced realistic surfaces in spite of their different texture characteristics. The 3D images of the fracture surfaces represent explicit information on the micro-macro structure. Therefore it can be claimed that material behavior is explicitly represented in the 3D image rather than the 2D image. This 3D image with texture representation indicates that the regions with a particular fracture and elevation texture (segments) did not behave like the rest of the material during the fracture process. Nevertheless, it is difficult to discuss the quality of the reconstructed surfaces at this level of magnification; therefore classical geometric case studies were tested and are described in the next section.

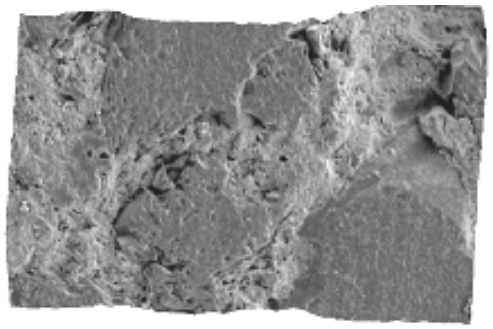

(a)

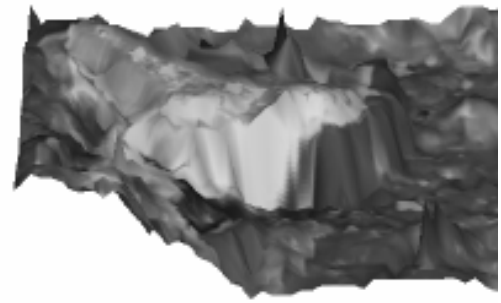

(b)

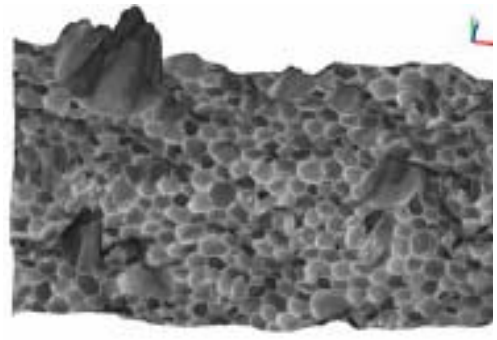

(c)

Figure 6: Reconstructed surfaces of: (a) ceramic material; (b) synthesis earth magma; and (c) syntactic foam.

Experiment	Tilt Angle	Magni-fication	Realistic Surface	Overlapping (Fracture closing)
Ceramic	10^4	X150	Yes	No
Magma	10^4	X2500	Yes	No
Syntactic Foam	10^4	X27	Yes	Yes

Table 1: Comparison between material samples.

4.2 Simulations of different geometries

Synthetic 3D geometric models with textures were created using CATIA CAD software. Cubes, cones and freeform surfaces were defined. The geometric models were reconstructed with complex synthetic textures because, according to the matching algorithm requirements, the intensity differentiation and texture must imitate micro-structures and be non-homogeneous. For example, for a uniform region within the pair of images, the algorithm will not be able to differentiate between the points inside this zone and therefore will fail to match the points.

Table 2 summarizes the error distribution of the different case studies of the geometric models. The simulation was based on the following stages:

a) The models were defined on the CAD system.

b) Two synthetic images were created for each model.

c) The proposed method was applied on these images and resulted in a 3D textured mesh.

d) The resulting 3D mesh was compared to the reference CAD model.

The CAD model and the resulting 3D mesh are represented by triangles. The distance error between the CAD and the reconstructed mesh was measured, indicating the number of triangles below 0.2%, 1.3% and 3%. The error of most of the models is less than 3%.

Relative Error / Study Case	<0.2%	<1.3%	<3%
Cube (front view)	24%	90%	100%
Cube (isometric)	43%	87%	99%
Freeform	0%	65%	85%

Table 2: Comparison between the geometric samples

Figure 7 demonstrates the distribution error of the geometric models. Figure 7.a shows the error distribution of a cube (front view), Figure 7.b demonstrates the error distribution of a cube (isometric) and Figure 7.c demonstrates the error distribution of a freeform surface.

4.3 Analyzing the surface roughness

A profile can be computed in any desired direction to analyze the roughness of the surface. The profile is obtained by computing the intersection of the surface with a given plane. Then, the profile curvature can be analyzed. Figure 8 demonstrates a profile that was extracted in a given direction.

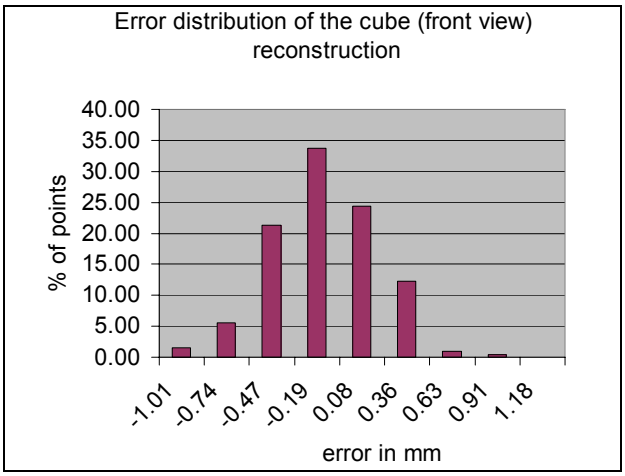

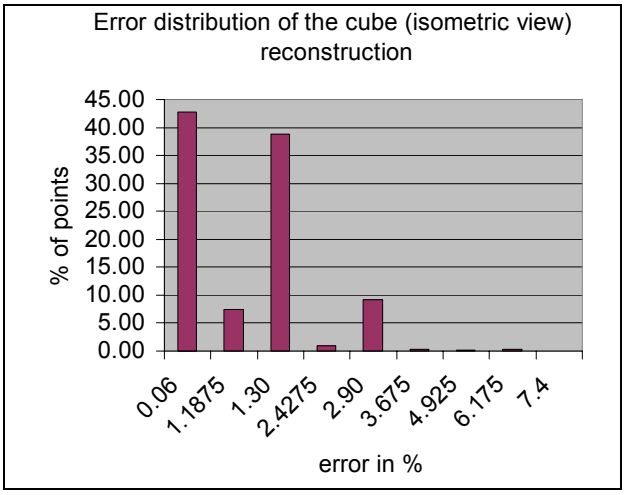

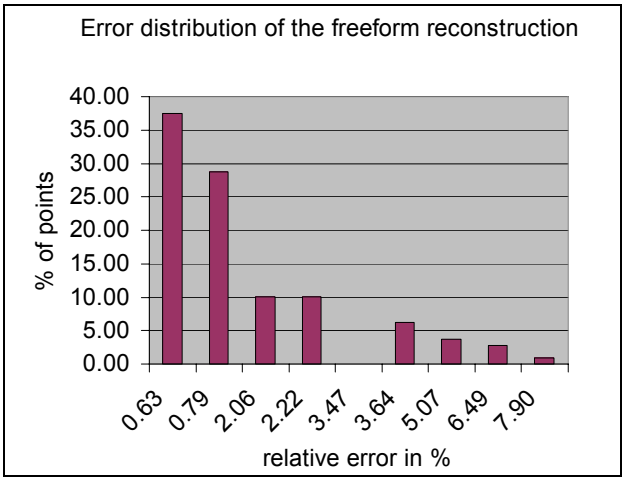

Figure 7: Error Distribution of two models: a cube (front and isometric views) and a freeform surface.

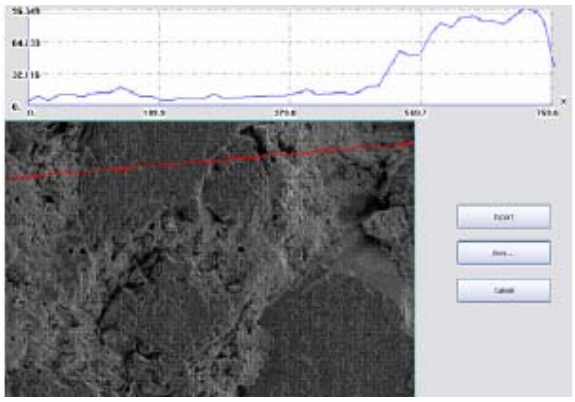

Figure 8: Roughness analysis: The 3D textured mesh and a profile of the roughness extracted in a given direction.

5 SUMMARY

A new method that reconstructs 3D textured meshes of macro-micro surfaces has been developed for 3D visualization and analysis. A set of 3D points is computed from two SEM images of a surface, and a 3D mesh is then reconstructed from the 3D points using the Delaunay triangulation. A very realistic surface is obtained by applying texture mapping on the mesh. Then, this 3D surface with texture is used for extracting profiles of the initial fracture surface. This approach was used to develop basic tools for the fractographic analysis domain, which are based upon texture analysis. By means of segmentation, it may be possible to partition the 3D surface into several segments characterized by their texture. These segments, based on their average weight, may yield specific mechanical features. The method has the following advantages:

- The method represents very realistic macro and micro structures simultaneously.
- The method enables mechanical 3D analysis.
- The method is simple to implement and fast.

This method has been applied to three fractured samples of ceramic material, magma and syntactic foam. The three materials present very different textures, and during the experiments, different magnifications were applied. Geometric CAD models, specifically a cube, a cone and freeform surface, were also tested using this method. Through the geometric CAD model reconstruction, the performance of the reconstruction process can be analyzed. The resulting points were compared to the original CAD model, and the errors were evaluated and discussed. The impact of some parameters on the reconstruction process was also evaluated. These analyses helped to validate the method. Nevertheless, the segmentation algorithms attempted in this research did not yield usable results.

6 ACKNOWLEGEMENTS

7 REFERENCES

[1] Evans, C., Bryan J., 1999, “Structured", "textured" or "engineered" surfaces, Annals of CIRP, 48/2:541-556.

[2] De Chiffre, L., Kunzmann, H., Peggs, G.N., Lucca, D.A., 2003, Surfaces in Precision Engineering, Microengineering and Nanotechnology, Annals of CIRP, 52/2:561-565.

[3] Bernard, A., Fischer, A., 2002, New Trends in Rapid Product Development, Annals of CIRP, 51/2:635-652.

[4] Stampfl, J., Scherer, S., Gruber, M., Kolednik, O., 1996, Reconstruction of Surface Topographies by Scanning Electron Microscopy for Application in Fracture Research, Appl. Phys. A: Mater. Sci. Process., 63/4:341-346.

[5] Barnard, S.T., Fischler, M.A., 1982, Computational Stereo, ACM Computing Surveys, 14:553-572.

[6] Azernikov, S., Miropolsky, A., Fischer, A., 2003, Surface Reconstruction of Freeform Objects Based on Multiresolution Volumetric Method, J. Comput. Inf. Sci. Eng. 3/4: 334-338.

[7] Klette, R., Rosenfeld, A., 2004, Digital Geometry - Geometric Methods for Digital Picture Analysis, Morgan & Kaufman, San Francisco.

[8] De Chiffre, L., Lonardo, P., Trumpold, H., Lucca, D.A., Goch, G., Brown, C.A., Hansen, H.N., 2000, Quantitative characterization of surface texture, Annals of CIRP, 49/2:635-652.

[9] Lonardo, P.M., Trumphold, H., De Chiffre, L., 1996, Progress in 3D Surface Micro-topography Characterisation, Annals of the CIRP, 45/2:589-593.

[10] Heckbert, P.S., 1986, Survey of texture mapping, IEEE Computer Graphics and Applications, 6/11:56-67.

[11] Harris C.G., Stevens, M.J., 1988, A Combined Corner and Edge Detector, Proc. of 4th Alvey Vision Conference.

[12] Kass, M., Witkin, A., Terzopoulos, D., 1988, Snakes: Active contour models, Int J Comput Vision, 321-331.

[13] Galun, M., Sharon, E., Basri, R., Brandt, A., 2003, Texture Segmentation by Multiscale Aggregation of Filter Responses and Shape Elements, IEEE Int. Conf. on Computer Vision (ICCV), Nice, 716-723.